Magn Reson Med Sci 2020; 19; 56–63
doi:10.2463/mrms.mp.2018-0144
Published Online: April 5, 2019

MAJOR PAPER

Signal Intensity within Cerebral Venous Sinuses on Synthetic MRI

Lydia Chougar[1,2], Akifumi Hagiwara[1,3*], Nao Takano[1], Christina Andica[1], Julien Cohen-Adad[1,4,5], Marcel Warntjes[6,7], Tomoko Maekawa[1,3], Masaaki Hori[1], Saori Koshino[1,3], Misaki Nakazawa[1], Osamu Abe[3], and Shigeki Aoki[1]

Purpose: Flowing blood sometimes appears bright on synthetic T_1-weighted images, which could be misdiagnosed as a thrombus. This study aimed to investigate the frequency of hyperintensity within cerebral venous sinuses on synthetic MR images and to evaluate the influence of increasing flow rates on signal intensity using a flow phantom.

Materials and Methods: Imaging data, including synthetic and conventional MRI scans, from 22 patients were retrospectively analyzed. Signal intensities at eight locations of cerebral venous sinuses on synthetic images were graded using the following three-point scale: 0, "dark vessel"; 1, "hyperintensity within the walls"; and 2, "hyperintensity within the lumen." A phantom with gadolinium solution inside a U-shaped tube was acquired without flow and then with increasing flow rates (60, 100, 200, 300, 400 ml/min).

Results: Considering all sinus locations, the venous signal intensity on synthetic T_1-weighted images was graded as 2 in 79.8% of the patients. On synthetic T_2-weighted images, all sinuses were graded as 0. On fluid-attenuated inversion recovery (FLAIR) images, sinuses were almost always graded as 0 (99.4%). In the phantom study, the signal initially became brighter on synthetic T_1-weighted images as the flow rate increased. Above a certain flow rate, the signal started to decrease.

Conclusion: High signal intensity within the cerebral venous sinuses is a frequent finding on synthetic T_1-weighted images. This corresponds to the hyperintensity noted at certain flow rates in the phantom experiment.

Keywords: *cerebral venous sinus, flow-related artifacts, synthetic magnetic resonance imaging, thrombosis*

Introduction

Signal analysis in vessels is often complex because of the variability in the appearance of flowing and stationary blood on MRI. Many technical factors affect the signal intensity of blood, including the type of sequence, sequence parameters, the field strength, and the use of flow-compensation techniques. Additionally, the signal intensity is also influenced by blood flow-related characteristics such as the direction of blood flow with respect to the B_0 field and the blood velocity, acceleration, and pulsatility.[1,2] Thus, rapidly flowing blood may cause a signal void, whereas slowly flowing blood may appear hyperintense and simulate a thrombus. Conversely, a thrombus may demonstrate variable MRI signals according to the stage of hemoglobin degradation.[2–4]

Synthetic MRI is a quantitative technique based on the absolute quantification of longitudinal relaxation time (T_1), transverse relaxation time (T_2), and proton density (PD), yielding a free range of contrast-weightings from a single acquisition, with high repeatability and reproducibility across

[1]Department of Radiology, Juntendo University School of Medicine, 1-2-1, Hongo, Bunkyo-ku, Tokyo 113-8421, Japan
[*]Corresponding author, Phone: +81-3-5802-1230, Fax: +81-3-3816-0958, E-mail: a-hagiwara@juntendo.ac.jp

Received: October 22, 2018 | Accepted: February 14, 2019

[2]Department of Radiology, Hôpital Cochin, Paris, France
[3]Department of Radiology, Graduate School of Medicine, The University of Tokyo, Tokyo, Japan
[4]NeuroPoly Lab, Polytechnique Montreal, Montreal, QC, Canada
[5]Functional Neuroimaging Unit, CRIUGM, Université de Montréal, Montreal, QC, Canada
[6]Center for Medical Imaging Science and Visualization (CMIV), Linköping University, Linköping, Sweden
[7]SyntheticMR AB, Linköping, Sweden

different vendors.[5,6] The quantification of relaxation times and proton density by multi-echo acquisition of a saturation recovery using turbo spin-echo readout (QRAPMASTER) pulse sequence, which is provided by the manufacturer SyntheticMR AB, Linköping, Sweden, is a two-dimensional multi-slice, multi-echo, and multi-saturation delay saturation recovery turbo spin-echo acquisition method that provides images for different combinations of TE and saturation delay time (TD). The acquired data are used to calculate T_1 and T_2 maps at each slice position, which are then used to extract the synthetic MR images.[6–10]

Theoretically, synthetic MRI based on QRAPMASTER is supposed to be an inherently black-blood imaging technique, due to the constant saturation of flowing blood, which implies that the vascular lumen is signal-free.[6] However, in our clinical experience, there are persistent flow-related artifacts in larger veins, especially on T_1-weighted images, rendering the vein lumen heterogeneous. This finding could raise a suspicion of venous thrombosis.

This study aimed to evaluate the signal intensity within cerebral venous sinuses (CVSs) on different contrast-weighted images obtained with synthetic MRI in a series of patients. We also performed experiments with a flow phantom to evaluate the effect of increasing flow rates on the signal intensity.

Materials and Methods

This retrospective study was approved by the Institutional Review Board of our institution. Written informed consent was not required for this study given its retrospective nature.

Patient data

The study population consisted of 22 consecutive patients (13 female and 9 male; average age, 57.3 years; age range, 27–85 years) who had undergone brain MRI studies at our institution in April 2015 for various indications (Table 1). All subjects fulfilled the following inclusion criteria: 1) availability of both conventional and synthetic MRI data and 2) no previous history of craniotomy, sinus thrombosis, or vascular malformation.

Table 1 Patient characteristics

Patient no.	Sex	Age (years)	Indication for MRI
1	F	43	RRMS, follow-up
2	F	53	Right optic neuritis, follow-up
3	M	75	Screening for cerebrovascular disease
4	F	36	RRMS, follow-up
5	M	71	Progressive dysarthria
6	F	40	Systemic lupus erythematosus, follow-up
7	M	70	Dementia
8	M	48	Intracranial hypertension, follow-up
9	F	85	Dementia
10	F	49	RRMS, follow-up
11	F	27	Pontomedullary junction tumor, follow-up
12	F	56	Dystonia
13	F	71	Screening of brain metastases
14	M	37	Angiitis of the central nervous system, follow-up
15	F	47	Left ICA dissecting aneurysm, follow-up
16	F	67	Screening for brain metastases
17	F	72	Old cerebral infarction, follow-up
18	M	79	Cerebellar ataxia
19	F	65	Old cerebral infarction, follow-up
20	M	52	Acute cerebral infarction, suspected
21	M	59	Screening for brain metastases
22	M	58	Acute cerebral infarction, suspected

Sex ratio: 1:4 (13 F, 9 M), Mean age: 57.3. "Follow-up" here indicates the patients did not have acute symptoms. F, female; ICA, intracranial artery; M, male; RRMS, relapsing-remitting multiple sclerosis.

Acquisition data

All MR examinations for patients were performed using a 3T MRI scanner (Discovery MR750w, GE Healthcare, Waukesha, WI, USA) with a 19-channel head coil. The protocol for conventional MRI sequences included T_1-weighted fast spin-echo inversion recovery, T_2-weighted periodically rotated overlapping parallel lines with enhanced reconstruction (PROPELLER), T_2^* gradient-echo, and fluid-attenuated inversion recovery (FLAIR) fast spin-echo sequences in the axial plane. The imaging parameters are summarized in Table 2.

Quantitative MRI was performed in addition to conventional MRI sequences using the QRAPMASTER sequence. Quantification map acquisition and raw data processing were performed with synthetic MRI software (v8.0, SyntheticMR AB), and synthetic images were created with the following parameters: TR = 500 ms and TE = 10 ms for T_1WI; TR = 4500 ms and TE = 100 ms for T_2WI; and TR = 15000 ms, TE = 100 ms, and TI = 3000 ms for FLAIR.

Data analysis

A radiology resident (L.C.) blinded to the clinical information performed readings of MRI scans based on T_1-weighted, T_2-weighted, and FLAIR images on synthetic MRI software for each patient. To evaluate interrater reliability, a senior

Table 2 Magnetic resonance imaging acquisition parameters

	T_1-weighted spin-echo IR[a]	T_2-weighted PROPELLER[a]	FLAIR[a]	T_2^* gradient-echo[a]	SyMRI[a]	SyMRI[b]
TR (ms)	3294.2	4500	9000	640	4000	4250
TE (ms)	17.15	110.16	121.63	15	16.9 and 84.5	22 and 99
TI (ms)	908	—	2637.1	—	—	—
FOV (cm^2)	24 × 27.8	24 × 24	24 × 24	24 × 18	24 × 24	23 × 18.6
Matrix	352 × 256	512 × 512	320 × 224	256 × 192	288 × 256	320 × 320
Section thickness (mm)	4	4	4	4	4	4
Gap (mm)	1	1	1	1	1	1
Number of sections	30	30	30	30	30	30
Number of average	1	1	1	1	1	1
Bandwidth (Hz/pixel)	300	195	280	230	31.25	150

SyMRI, synthetic MRI; [a]Discovery MR750w, GE Healthcare; [b]MAGNETOM Prisma, Siemens Healthineers. TI, inversion delay.

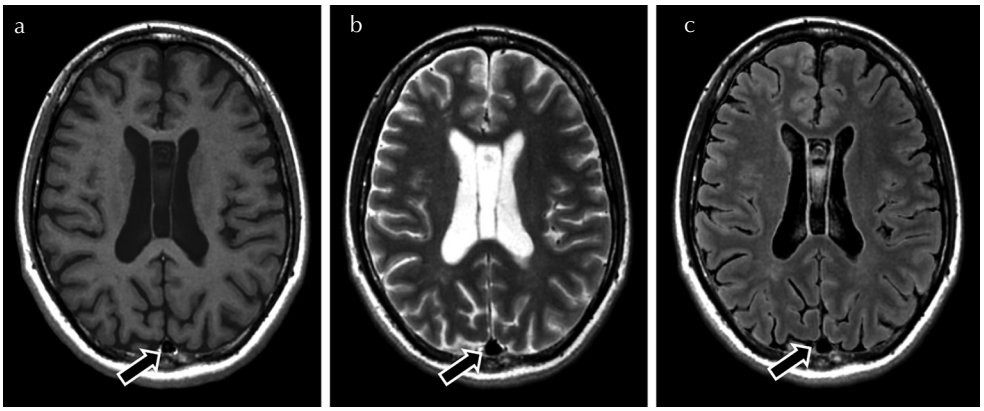

Fig. 1 Illustration of a grade 1 signal intensity within the superior sagittal sinus (arrow) on synthetic T_1-weighted images (**a**). The sinus is scored as 0 on T_2-weighted (**b**) and FLAIR (**c**). FLAIR, fluid-attenuated inversion recovery.

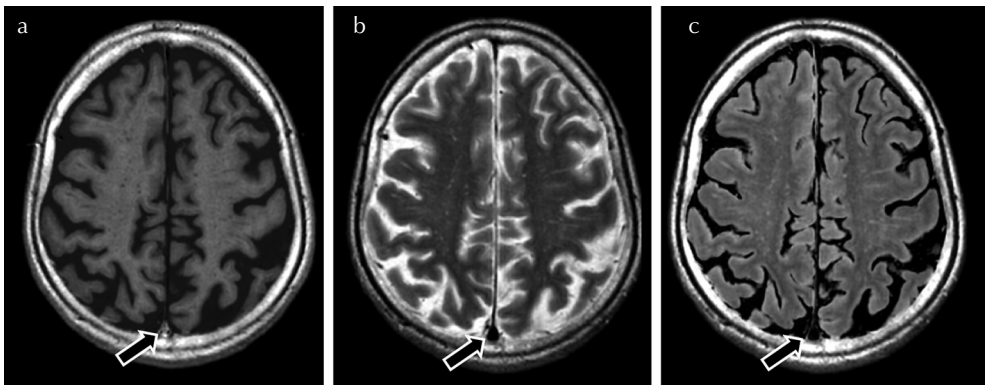

Fig. 2 Illustration of a grade 2 signal intensity within the superior portion of the superior sagittal sinus (arrow) on synthetic T_1-weighted images (**a**). The sinus (arrows) is scored as 0 on T_2-weighted images (**b**) and FLAIR images (**c**). FLAIR, fluid-attenuated inversion recovery.

neuroradiologist (C.A.) conducted a second reading of the same imaging dataset.

The signal intensities at different locations within the CVS lumen were rated using a three-point scale, with 0 indicating "vessel completely dark," 1 indicating "hyperintensity within the walls sparing the lumen" (Fig. 1), and 2 indicating "hyperintensity within the lumen" (Fig. 2). For each sinus, the first rater designated a reference slice that the second rater read subsequently.

The following eight venous segments were analyzed: two sites in the superior sagittal sinus (the convexity and the level of the bodies of the lateral ventricles), straight sinus (the level of the foramen of Monro), confluence of sinuses, right transverse sinus, right sigmoid sinus, left transverse sinus, and left sigmoid sinus. When a sinus was hypoplastic, the signal intensity was not evaluated. Additionally, the signal intensities within the petrous internal carotid arteries (at the end of the horizontal portion) were analyzed using the same scale.

The presence of ghosting artifacts near the different venous segments was also investigated.

Conventional MR images were analyzed in search of sinus abnormalities suggestive of thrombus, such as sinus enlargement or focal areas with blooming artifacts. Follow-up conventional MRI scans performed between 4 and 33 months after the initial examination, depending on the subjects, were available in 15 patients. T_1-weighted sequence with administration of gadolinium-based contrast agent was not available for all patients at the time of the examination or in the further studies. Medical charts of all patients were consulted.

Phantom study

A flow water phantom (HB-1; FUYO-CORPORATION, Tokyo, Japan) was scanned using a 3T unit (MAGNETOM Prisma; Siemens Healthineers, Erlangen, Germany) with a 64-channel head coil. A QRAPMASTER pulse sequence was acquired. Patients and the phantom were scanned on different machines because the GE scanner was not available at the time of phantom acquisition for organizational reasons. The sequence parameters for the GE and Siemens scanners were virtually identical, as provided by the manufacturer (Synthetic MR AB). We used the same post-processing parameters for these two scanners. Synthetic T_1- and T_2-weighted images and T_1, T_2, and PD maps obtained from the QRAPMASTER sequence were analyzed.

The flow apparatus consisted of a U-shaped tube with two straight portions connected by a curved portion. The inner and outer diameters of the tube were 5 and 8 mm, respectively. The distance between the left and right tubes was 6 cm. The straight portion of the tubes was 30 cm long. The phantom was immersed in a static half-filled water bath. The flow rate through the tubes was monitored continuously using a calibrated flow pump (ALPHA FLOW EC-1, FUYO-CORPORATION) (Fig. 3). The recirculating fluid was a gadolinium solution (ProHance; Bracco-Eisai, Tokyo, Japan) diluted to mimic the T_1-relaxation time of blood (1500 ms).[11] The room temperature was kept at 20.8°C.

The flow apparatus was placed within the magnet so that the flow directions were parallel to the magnet bore. The phantom was scanned in an axial plane, without flow, and then with a steady flow at different rates (60, 100, 200, 300, 400 ml/min). Mean flow velocities were calculated using the following formula:

$$V = Q/S = Q/\pi r^2,$$

where V is the blood velocity in cm/s; Q, the flow rate in ml/s or cm^3/s; S, the area of the vessel section in cm^2; and r, the radius in cm. Thus, the corresponding mean flow velocities were 5.1, 8.5, 17.0, 25.5, and 34.0 cm/s, respectively. These values were set to cover the physiological variability of flow velocities (i.e., mean velocities = 6–13 cm/s and peak velocities = 16–32 cm/s) in a healthy population in different locations of the CVS, as described previously.[12] The solution flowed into the left segment of the tube and out from the right segment. Phase-encoding was oriented in the anteroposterior axis to avoid projection of pulsation artifacts on the adjacent tube. No flow-compensation technique or presaturation pulses were used.

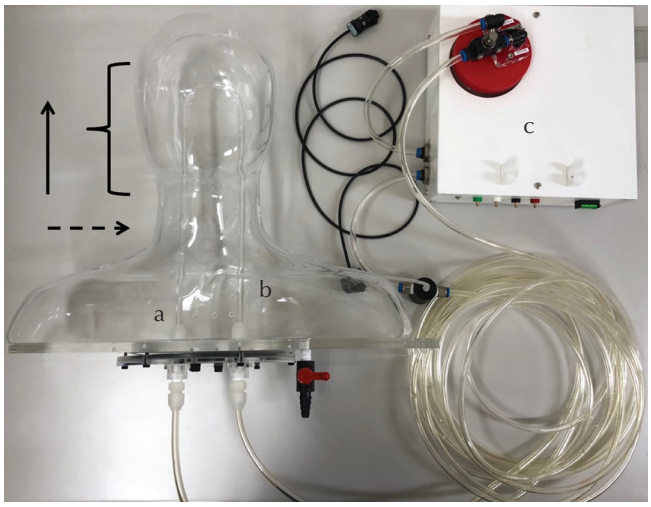

Fig. 3 Configuration of the flow phantom apparatus. The flow phantom consists of a U-shaped tube with two straight portions connected by a curved portion. The solution flows into segment (**a**) and out from segment (**b**). They are connected to the calibrated flow pump (**c**) that monitors the flow rates. The solid arrow represents the direction of the magnetic field B_0. The curly bracket indicates the acquisition volume. The dashed arrow represents the acquisition plane.

The phantom was scanned three times without flow and twice with flow. Signal intensity and quantitative parameters were analyzed at the same slice between the different acquisitions, at the level of the middle portion of the tube. The choice of this central slice, distant from possible artifacts occurring at the extremities of the phantom, was assumed to be more representative. The ROI analysis on images without flow were based on the three acquisitions, with one ROI for each acquisition. With flow, we showed the results obtained with the acquisition which was less subjected to flow artifacts. We did not provide quantitative measurements as the values were quite variable within the lumen (in the same slice and through different slices).

Statistical analysis

An interrater reliability coefficient was calculated using squared weighted Cohen's Kappa test after pooling the results from the three sequences and considering all the locations of sinuses for all the patients. A value <0.2 indicated very poor agreement; 0.2–0.4, slight agreement; 0.4–0.6, moderate agreement; 0.6–0.8, substantial (good, high) agreement; and values >0.8, excellent agreement. Statistical analyses were performed using the software package R version 3.2.1 (http://www.R-project.org/)

Results

Patient data

Considering all CVSs, on synthetic T_1-weighted images, the venous signal intensity was bright (rated grade 2) in 79.8% of the patients. Grade 1 was observed in 19% of the patients (Table 3). Conversely, on synthetic T_2-weighted images, sinuses were always dark (grade 0). On FLAIR images, the signal was almost always low (99.4% for grade 0). Details of the grading for each sinus are shown in Table 3.

Considering the petrous internal carotid arteries, grade 0 was noted in 77%, 95%, and 95% of the patients on synthetic T_1-weighted, T_2-weighted, and FLAIR images, respectively. No patient showed grade 2 findings. Considering the three synthetic images and all locations of sinuses for all patients (a total of 489 values), the agreement was almost perfect, with a squared weighted Cohen's Kappa coefficient equal to 0.967 ($P < 0.05$).

No major ghosting artifact near the CVS was seen on any of the synthetic images. On conventional MR images, no sinus abnormality suggestive of thrombosis was observed in any of the patients. Assessments of follow-up MRI studies as well as the medical file did not show any finding indicating CVS thrombosis.

Phantom study

Without flow, the signal intensities within the tubes were homogeneous, appearing moderately hyperintense on both T_1- and T_2-weighted images (Fig. 4). On T_1-weighted images, at a flow rate of 60 ml/min, the lumen in the inflow tube appeared dark and surrounded by a thin hyperintense rim. The results below were obtained with the acquisition which was less subjected to flow artifacts. At 100 ml/min, a slightly hyperintense spot appeared in the center, displaying a "target" appearance. No significant pulsation artifact was seen. At 200 ml/min, the lumen became slightly brighter while ghosting artifacts in the anteroposterior axis appeared. At 300 ml/min, the signal was heterogeneous, partly bright. At 400 ml/min, the heterogeneity and ghosting artifacts decreased. On T_2-weighted images, the signal intensity immediately decreased and remained low, with pulsation artifacts being much less visible on T_2-weighted images compared with T_1-weighted images.

On T_1-weighted images, at a flow rate of 60 ml/min, the signal intensity in the outflow tube became bright and heterogeneous and ghosting artifacts appeared. The signal intensity continued to increase at 100, then 200 ml/min. At 300 ml/min, and then at 400 ml/min, the signal intensity started to decrease along with a marked reduction of the pulsation artifacts. On T_2-weighted images, the signal intensity

Table 3 Analysis of the CVS signal intensity on synthetic T_1-weighted, T_2-weighted, and FLAIR images for all the patients for each location

	T_1-weighted images (%)			T_2-weighted images (%)			FLAIR images (%)		
SSS	0	1	2	0	1	2	0	1	2
Convexity	0/22	5/22 (23)	17/22 (77)	22/22 (100)	0/22	0/22	22/22 (100)	0/22	0/22
LV	0/22	2/22 (9)	20/22 (91)	22/22 (100)	0/22	0/22	22/22 (100)	0/22	0/22
SS	2/22 (9)	15/22 (68)	5/22 (23)	22/22 (100)	0/22	0/22	22/22 (100)	0/22	0/22
Confluence	0/22	1/22 (5)	21/22 (95)	22/22 (100)	0/22	0/22	22/22 (100)	0/22	0/22
Right TS*	0/19	1/19 (5)	18/19 (95)	19/19 (100)	0/19	0/19	19/19 (100)	0/19	0/19
Left TS*	0/14	1/14 (7)	13/14 (93)	14/14 (100)	0/14	0/14	14/14 (100)	0/14	0/14
Right SigS	0/21	2/21 (10)	19/21 (90)	22/21 (100)	0/21	0/21	21/21 (100)	0/21	0/21
Left SigS*	0/21	4/21 (19)	17/21 (81)	21/21 (100)	0/21	0/21	20/21 (95)	1/21 (5)	0/21
Including all the locations of CVS*	2/163 (1.2)	31/163 (19)	130/163 (79.8)	163/163 (100)	0/163	0/163	162/163 (99.4)	1/163 (0.6)	0/160
ICA	17/22 (77)	5/22 (23)	0/22	21/22 (95)	1/22 (5)	0/22	21/22 (95)	1/22 (5)	0/22

*The right and left transverse sinuses were hypoplastic in three and eight patients, respectively. The right and left sigmoid sinuses were hypoplastic in one and one patient. CVS, cerebral venous sinus; ICA, internal carotid artery (petrous segment); LV, lateral ventricles; SSS, superior sagittal sinus; SS, straight sinus; SigS, sigmoid sinus; TS, transverse sinus.

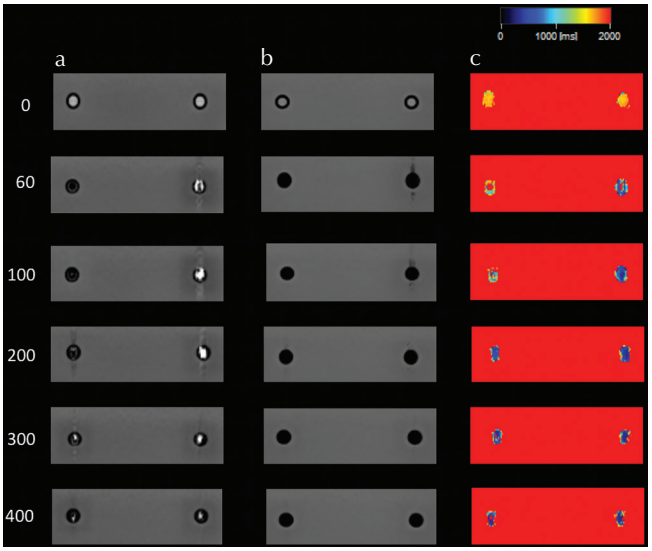

Fig. 4 Flow phantom study. Evolution of signal intensity through different flow rates on synthetic T_1- (row **a**) and T_2-weighted (row **b**) images in the axial plane. The same slice is displayed for each figure. The flowing solution enters the left segment of the tube and exits from the right segment. Row **c** shows the corresponding T_1 maps. On T_1-weighted images, the signal intensity first increases in both segments along with pulsation artifacts. Then above a certain flow rate, the signal starts to decrease.

immediately decreased and remained low while the flow rate increased. The signal intensity increase with flow velocities, as well as the pulsation artifacts, were much more prominent in the outflow tube than the inflow tube.

Considering the quantitative parameters, without flow, the T_1, T_2 and PD values obtained were similar between the three acquisitions. Mean ± standard deviation (SD) were equal to 1724 ± 67, 1651 ± 230 ms, and 107 ± 1% in the inflow tube and 1697 ± 61 ms, 1778 ± 148, and 107 ± 2% in the outflow tube, respectively, based on the three acquisitions.

With flow, an overall decrease of T_1, T_2, and PD values could be visually assessed on each quantitative map, even though there was a great dispersion of the values, making measurements inaccurate (Fig. 4).

Discussion

Synthetic MRI based on the QRAPMASTER pulse sequence is considered a black-blood imaging technique because of the constant saturation of flowing blood.[6] However, we assessed the frequency of high signal intensities within CVSs on synthetic T_1-weighted images, since such findings could raise suspicion of venous thrombosis.

Indeed, in the acute stage of thrombosis (within 7 days following the onset of the symptoms), the thrombus is initially isointense on spin-echo T_1-weighted images and hypointense on T_2-weighted images due to paramagnetic properties of deoxyhemoglobin. In the subacute stage, it becomes hyperintense on both T_1- and T_2-weighted images owing to the presence of extracellular methemoglobin. The thrombus can occasionally appear hyperintense on T_1-weighted images and hypointense on T_2-weighted images due to the presence of intracellular methemoglobin,[3] leading to the risk of misdiagnosing a venous T_1-weighted hyperintensity as a thrombus. Given the retrospective nature of our study and the low pre-test probability of thrombosis, this diagnosis could be easily ruled out by a cross-comparison with other weightings on conventional and synthetic MRI along with the clinical and follow-up imaging data. Nevertheless, the distinction can be more difficult in routine MRI evaluations. The pre-test probability based on the symptomatology, the patient history, and the risk factors for thrombosis should help radiologists in this interpretation.

Although synthetic MRI has demonstrated clinical accuracy in various neurological processes, it has some pitfalls.[13] Concerning flow effects, Lee et al.[14] reported an increase in pulsation artifacts caused by arteries and cerebrospinal fluid on synthetic non-enhanced T_1-weighted images in comparison with conventional T_1-weighted images in children over 2 years of age (until 16 years). To the best of our knowledge, no study has ever analyzed the signal intensity within CVSs on synthetic MRI.

The flow phantom experiment in our study showed that when a solution was flowing in or out of the tube, the signal was prone to become bright on synthetic T_1-weighted images as the flow rate increased. The flowing fluid within the phantom would be presumed to have a lamellar profile, consequently explaining the difference of appearance between the periphery of the lumen which was dark, and the center which was bright, as the center will flow faster. Signal changes were much more important in the outflow segment of the phantom rather than in the inflow segment. These differences are likely to be linked with flow direction. Interestingly, the signal started to decrease above a certain flow rate (300 ml/min for the inflow tube; 200 ml/min for the outflow tube). Thus, the signal intensity may have continued to decrease for higher velocities, representative of arteries. Indeed, the normal velocities of cerebral arteries (peak and mean) are higher than the highest value used in our phantom experiment (33.3 cm/s).[15] These observations were consistent with the high frequency of hyperintensity within CVSs in the patients' MRI scans. Conversely, the signal within cavernous internal carotid arteries was more often dark on synthetic T_1-weighted images, only displaying a thin peripheral hyperintensity in less than a quarter of the patients. Our investigations also revealed that the signal within both CVSs and tubes always remained dark on synthetic T_2-weighted images, this contrast-imaging being much less sensitive to pulsation artifacts than T_1-weighted images.

The behavior of flowing blood signals on MRI sequences is complex and responds to intricate technical and physiological factors. Imaging factors include the type of sequence, the sequence parameters, the field strength, and the use of flow-compensation techniques and cardiac and/or respiratory gating.[1,4] Various blood flow-related characteristics such as

the mean and the peak blood velocities, the distribution of the velocities, the acceleration, the pulsatility and the direction and orientation of the flowing blood with respect to the B_0 field, should also be considered.

Time-of-flight effects affect the vessel's signal on spin-echo sequences differently according to the blood velocities, with respect to the imaging parameters. They proceed from the motion of protons flowing in or out of an imaging volume. At low velocities, the signal intensity is high and first gradually increases with velocity until a peak velocity is reached. Indeed when unsaturated blood enters the imaged volume and is subject to its first set of pulses, it will generate a stronger signal compared with stationary tissues: this is the "flow-related enhancement", also known as the "entry phenomenon." It is typically seen at the first slices of a multislice acquisition. If blood flow is sufficiently rapid, the effect may penetrate several slices deep into the volume. The effect is maximal when blood flows perpendicular to the image plane.[2] The use of a presaturation pulse, with a band being positioned at the top or at the bottom at the imaging volume, suppresses the flow-related enhancement effect by saturating the moving spins that were initially out of the image volume.[16] This "flow-related enhancement" phenomenon might account for the increase in signal intensity initially observed within the inflow segment. The signal within the outflow tube was also mainly bright although it would be expected to be low owing to the saturation of spins. Hence the magnetization state of flowing spins might have changed while passing through the curved portion of the tube, which was included in the acquisition volume. The hyperintensity observed in the outflow tube could be explained by the assumption that the spins had enough time to recover their longitudinal magnetization before arriving in the outflow segment, thus generating a high signal. It is difficult to say to what extent the geometry of the tube, especially the length of the U-shaped portion, might have influenced these signal's changes.

In the second phase, at higher velocities, the signal gradually decreases when a maximal speed is reached.[2] It is known that spins rapidly flowing out of slices that have received the 90° pulse can miss the 180° pulse. They are replaced by protons that were not exposed to the 90° pulse and thus do not have any transversal magnetization, resulting in a low signal. This second type of time-of-flight effect could account for the decrease in signal intensity observed within the phantom on T_1-weighted images at high velocities. Furthermore high-velocity signal loss is more prominent on long TE spin-echo images since long echo times provide a greater chance for spins to flow out of the slice between the 90° and 180° pulses.[2,17,18] This could explain why vessels are more prone to appear black on T_2-weighted images than T_1-weighted images. With gradient-echo sequences, only flow-related enhancement is seen. High-velocity signal loss does not occur since the read-out gradient which forms the echo in gradient-echo images is not slice selective.[2,17,18] However, one should keep in mind that flow effects in synthetic MRI are more complex than in conventional spin- or gradient-echo sequences. The behavior of flowing blood is more difficult to predict because synthetic MRI involves quantification of T_1, T_2, and PD, and synthesis of contrast-weighted images is based on multiple raw images without consideration of flow effects.

On the other hand, spin-phase effects refer to changes in the precession angle of protons while moving within a gradient. If a proton changes its position while the gradients are applied, it will lose phase compared with stationary tissues, inducing a vascular signal loss. Spin-phase effects are particularly visible near vessel walls and in the regions of turbulence.[1,17] They might account for the signal loss observed with higher velocities. Gradient-moment nulling or flow-compensation gradients can reduce flow-related artifacts by compensating for the spin-phase dispersion due to the movement of flowing protons.[19] Flow-compensation gradient techniques are not implemented in the QRAPMASTER sequence used at our institution. The influence of flow-compensation techniques on vessels signal would be an interesting parameter to explore in future works.

Limitations

There are several limitations to our study. First, the pre-test probability of venous thrombosis in our series of patients was low, with patients being referred for various indications. Selecting a target population with a clinical suspicion of deep venous thrombosis would have been more relevant. However, such patients were not available in our database.

Second, our study focused on CVS signals. For arteries, signal analysis was limited to one location. Even though no patient showed hyperintensity in the lumen of the internal carotid arteries, a more exhaustive reading, including many arterial locations, would have been more accurate. Nevertheless, the signal-intensity scoring was difficult owing to the partial volume effects generated by a small arterial caliber and frequent changes in direction.

Third, our flow phantom experiment did not take into account the pulsatile behavior seen in veins. Indeed, similar to arteries, CVSs also display a degree of pulsatility mainly attributable to arterial pulsations passively transmitted to the venous system.[1,2,20,21] As shown by Stoquart-Elsankari et al.,[20] the pulsatility index (represented by the difference between the maximum and the minimum velocities divided per the maximum velocity, multiplied by 100) was lower in the superior sagittal sinus (21 ± 10) than the internal jugular vein (38 ± 15). Further studies should evaluate the effect on the signal intensity of a pulse applied to a flowing solution.

Another physiological condition influencing venous flow is breathing. Using MR venography and phase-contrast images with peripheral pulse gating, Kudo et al.[22] showed that breath-holding affects signal intensities and blood velocities in a series of patients. In our study, technical limitations did not allow this parameter to be implemented in the phantom experiment.

Conclusion

Our study showed that CVSs often show a high intraluminal signal on synthetic T_1-weighted sequences. This could be a pitfall of synthetic MRI and should not be misdiagnosed as venous thrombosis. The clinical findings correlated with the experimental observations, wherein the signal intensity within the outflow tube increased when flow was added to the solution.

Funding

This work was supported by the Japan Society for the Promotion of Science (JSPS) KAKENHI (grant number 16K19852); by a JSPS Grant-in-Aid for Scientific Research on Innovative Areas, resource and technical support platforms for promoting research Advanced Bioimaging Support (grant number JP16H06280); by the Japan Radiological Society and Bayer Yakuhin (KJ-08); and by the Impulsing Paradigm Change through Disruptive Technologies (ImPACT) Program of the Council for Science, Technology and Innovation (Cabinet Office, Government of Japan).

Conflicts of Interest

Marcel Warntjes is currently employed part-time at SyntheticMR and has stocks in SyntheticMR. The other authors do not have any conflicts of interest to disclose.

References

1. von Schulthess GV, Higgins CB. Blood flow imaging with MR: spin-phase phenomena. Radiology 1985; 157: 687–695.
2. Axel L. Blood flow effects in magnetic resonance imaging. AJR Am J Roentgenol 1984; 143:1157–1166.
3. Ihn K, Jung WS, Hwang SS. The value of T_2^*-weighted gradient echo MRI for the diagnosis of cerebral deep venous thrombosis. Clin Imaging 2013; 37:446–450.
4. Nadel L, Braun IF, Kraft KA, Fatouros PP, Laine FJ. Intracranial vascular abnormalities: value of MR phase imaging to distinguish thrombus from flowing blood. AJR Am J Roentgenol 1991; 156:373–380.
5. Hagiwara A, Hori M, Cohen-Adad J, et al. Linearity, bias, intrascanner repeatability, and interscanner reproducibility of quantitative multidynamic multiecho sequence for rapid simultaneous relaxometry at 3 T: a validation study with a standardized phantom and healthy controls. Invest Radiol 2019; 54:39–47.
6. Warntjes JB, Leinhard OD, West J, Lundberg P. Rapid magnetic resonance quantification on the brain: optimization for clinical usage. Magn Reson Med 2008; 60: 320–329.
7. Hagiwara A, Hori M, Yokoyama K, et al. Synthetic MRI in the detection of multiple sclerosis plaques. AJNR Am J Neuroradiol 2017; 38:257–263.
8. Hagiwara A, Nakazawa M, Andica C, et al. Dural enhancement in a patient with Sturge–Weber syndrome revealed by double inversion recovery contrast using synthetic MRI. Magn Reson Med Sci 2016; 15:151–152.
9. Wallaert L, Hagiwara A, Andica C, et al. The advantage of synthetic MRI for the visualization of anterior temporal pole lesions on double inversion recovery (DIR), phase-sensitive inversion recovery (PSIR), and myelin images in a patient with CADASIL. Magn Reson Med Sci 2018; 17:275–276.
10. Andica C, Hagiwara A, Nakazawa M, et al. Synthetic MR imaging in the diagnosis of bacterial meningitis. Magn Reson Med Sci 2017; 16:91–92.
11. Lu H, Clingman C, Golay X, van Zijl PC. Determining the longitudinal relaxation time (T_1) of blood at 3.0 Tesla. Magn Reson Med 2004; 52:679–682.
12. Schuchardt F, Schroeder L, Anastasopoulos C, et al. In vivo analysis of physiological 3D blood flow of cerebral veins. Eur Radiol 2015; 25:2371–2380.
13. Tanenbaum LN, Tsiouris AJ, Johnson AN, et al. Synthetic MRI for clinical neuroimaging: results of the magnetic resonance image compilation (MAGiC) prospective, multicenter, multireader trial. AJNR Am J Neuroradiol 2017; 38:1103–1110.
14. Lee SM, Choi YH, Cheon JE, et al. Image quality at synthetic brain magnetic resonance imaging in children. Pediatr Radiol 2017; 47:1638–1647.
15. Demirkaya S, Uluc K, Bek S, Vural O. Normal blood flow velocities of basal cerebral arteries decrease with advancing age: a transcranial Doppler sonography study. Tohoku J Exp Med 2008; 214:145–149.
16. Ehman RL, Felmlee JP. Flow artifact reduction in MRI: a review of the roles of gradient moment nulling and spatial presaturation. Magn Reson Med 1990; 14:293–307.
17. Urchuk SN, Plewes DB. Mechanisms of flow-induced signal loss in MR angiography. J Magn Reson Imaging 1992; 2:453–462.
18. Bradley WG, Waluch V, Lai KS, Fernandez EJ, Spalte C. The appearance of rapidly flowing blood on magnetic resonance images. AJR Am J Roentgenol 1984; 143:1167–1174.
19. Quencer RM, Hinks AS, Pattany PH, Horen M, Post MJ. Improved MR imaging of the brain by using compensating gradients to suppress motion-induced artifacts. AJR Am J Roentgenol 1988; 151:163–170.
20. Stoquart-Elsankari S, Lehmann P, Villette A, et al. A phase-contrast MRI study of physiologic cerebral venous flow. J Cereb Blood Flow Metab 2009; 29:1208–1215.
21. Shaller B. Physiology of cerebral venous blood flow: from experimental data in animals to normal function in humans. Brain Res Rev 2004; 46:243–260.
22. Kudo K, Terae S, Ishii A, et al. Physiologic change in flow velocity and direction of dural venous sinuses with respiration: MR venography and flow analysis. AJNR Am J Neuroradiol 2004; 25:551–557.